HHS Public Access

Author manuscript

Neuroimage. Author manuscript; available in PMC 2015 October 01.

Published in final edited form as:

Neuroimage. 2014 October 1; 99: 256–268. doi:10.1016/j.neuroimage.2014.05.036.

Contributors to contrast between glioma and brain tissue in chemical exchange saturation transfer sensitive imaging at 3 Tesla

Rachel Scheidegger[a,b], **Eric T Wong**[c,d], and **David C Alsop**[b,e]

Rachel Scheidegger: rscheide@mit.alum.edu; Eric T Wong: ewong@bidmc.harvard.edu; David C Alsop: dalsop@bidmc.harvard.edu

[a]Harvard-MIT Division of Health Sciences and Technology, 77 Massachusetts Ave E25, Cambridge, MA 02139, USA

[b]Radiology, Beth Israel Deaconess Medical Center, 330 Brookline Ave, Boston, MA 02215, USA

[c]Brain Tumor Center & Neuro-Oncology Unit, Beth Israel Deaconess Medical Center, 330 Brookline Ave, Boston, MA 02215, USA

[d]Neurology, Harvard Medical School, Boston, MA 02115, USA

[e]Radiology, Harvard Medical School, Boston, MA 02115, USA

Abstract

Off-resonance saturation transfer images have shown intriguing differences in intensity in glioma compared to normal brain tissues. Interpretation of these differences is complicated, however, by the presence of multiple sources of exchanging magnetization including amide, amine, and hydroxyl protons, asymmetric magnetization transfer contrast (MTC) from macromolecules, and various protons with resonances in the aliphatic spectral region. We report a study targeted at separating these components and identifying their relative contributions to contrast in glioma. Off-resonance z-spectra at several saturation powers and durations were obtained from 6 healthy controls and 8 patients with high grade glioma. Results indicate that broad macromolecular MTC in normal brain tissue is responsible for the majority of contrast with glioma. Amide exchange could be detected with lower saturation power than has previously been reported in glioma, but it was a weak signal source with no detectable contrast from normal brain tissue. At higher saturation powers, amine proton exchange was a major contributor to the observed signal but showed no significant difference from normal brain. Robust acquisition strategies that effectively isolate the contributions of broad macromolecular MTC asymmetry from amine exchange were demonstrated that may provide improved contrast between glioma and normal tissue.

Correspondence to: David C. Alsop, Beth Israel Deaconess Medical Center, 330 Brookline Ave, Ansin 226, Boston, MA 02215, Tel: 617 667-0275, Fax: 617 667-7917, dalsop@bidmc.harvard.edu.

Keywords

APT - Amide proton transfer imaging; CEST – chemical exchange saturation transfer; z-spectroscopy; NOE – nuclear overhauser effect; SAFARI – saturation with alternating frequency RF irradiation; MT, MTC – magnetization transfer contrast; magnetization transfer asymmetry; brain tumors; glioma; glioblastoma

Introduction

Off-resonance saturation transfer imaging methods, such as magnetization transfer (MT) imaging (Henkelman et al., 2001; Wolff and Balaban 1989) and chemical exchange saturation transfer (CEST) imaging (van Zijl and Yadav 2011; Ward et al., 2000; Zhou and van Zijl 2006), have been used increasingly for the study of brain tumors. Saturation transfer imaging at the amide proton frequency (3.5ppm), known as amide proton transfer (APT) (van Zijl et al., 2003; Zhou et al., 2003b) imaging, is thought to generate MRI contrast related to pH and the protein content inside cells. It has emerged as a potentially important tool for localizing tumors both in animal models (Salhotra et al., 2008; Zhou et al., 2003a) and humans (Jia et al., 2011; Jones et al., 2006; Wen et al., 2010; Zhao et al., 2012), and for grading (Zhou et al., 2008) brain tumors. It has also shown promise at evaluating tumor treatment response, as it may distinguish tumor recurrence from radiation necrosis (Wang et al., 2012; Zhou et al., 2011), which otherwise can appear similar on magnetic resonance images. Though the origin of the saturation transfer signal in tumors has not been fully explained, it has been attributed to increased mobile protein concentrations in malignant cells (Jones et al., 2006; Wen et al., 2010; Zhou et al., 2003a; Zhou et al., 2008; Zhou et al., 2011).

Despite the initial success of brain tumor imaging with saturation transfer imaging, isolating the contribution of amide proton concentration to the contrast remains difficult. It is well known that the off-resonance RF irradiation used to generate the APT signal also induces direct water saturation (DS) and broad macromolecular magnetization transfer contrast (MTC). These effects are typically removed by magnetization transfer ratio asymmetry (MTR_{asym}) analysis, where an image acquired with saturation at the amide proton frequency is subtracted from a control image acquired with RF saturation on the opposite side of the water line. MTR_{asym} analysis, however, introduces further sources of errors due to the asymmetric macromolecular MTC effect (Hua et al., 2007b; Pekar et al., 1996; Stein et al., 1994) and the presence of saturation peaks attributed to aliphatic protons in a frequency range from approximately -1 ppm to -5 ppm (Avni et al., 2009; Jin et al., 2012a; Jin et al., 2012b; Jones et al., 2012; Ling et al., 2008; Mori et al., 1998; Mougin et al., 2010; Narvainen et al., 2010; van Zijl et al., 2003; Wüthrich 1986; Zhou et al., 2003b). Note that aliphatic protons are believed to exchange magnetization through nuclear Overhauser enhancement (NOE) (Wüthrich 1986; Zhou et al., 2003b), rather than chemical exchange. As a result of these two confounds, MTR_{asym} values at 3.5ppm are negative in normal tissue when saturation powers less than 2 μT are employed. In order to account for these negative sources of saturation transfer, the MTR_{asym} parameter has been broken up into two components (Zhou et al., 2003b):

$$MTR_{asym}(\omega) = MTR'_{asym}(\omega) + APTR(\omega) \quad [1]$$

where APTR is the proton transfer ratio from amide protons and MTR'_{asym} incorporates negative sources of saturation transfer and errors.

One approach proposed to remove the undesired contributions of MTR'_{asym} to MTR_{asym} and isolate the APT effect is to subtract the asymmetry of a control region from the diseased region (Salhotra et al., 2008; Zhao et al., 2011; Zhou et al., 2003a):

$$\begin{aligned}\Delta MTR_{asym}(\omega) &= MTR_{asym}(\omega, \text{disease}) - MTR_{asym}(\omega, \text{control}) \\ &= \Delta MTR'_{asym}(\omega) + \Delta APTR(\omega)\end{aligned} \quad [2]$$

If MTR'_{asym}, which includes the NOE from aliphatic peaks and macromolecular MTC asymmetry, is unchanged between regions ($\Delta MTR'_{asym} = 0$), the subtraction will eliminate the negative contribution to the asymmetry and yield the desired APT effect. The assumption of constant MTR'_{asym} in cancer has not been verified, however, and may be suspect.

In addition to the negative MTR'_{asym} contributions from MTC asymmetry and aliphatic protons, fast exchanging amine and hydroxyl protons may also introduce errors to the saturation transfer measurement of amide protons at 3.5ppm. While amine protons resonate in a frequency range from 2–3ppm, recent saturation transfer studies both in phantoms and in-vivo have shown that the amine CEST peak is much broader and contributes significant signal at 3.5ppm when high saturation powers are employed (Cai et al., 2012; Jin et al., 2012b; Kogan et al., 2013). Given the multiple different sources of saturation transfer present at +/−3.5ppm it is unclear whether amide protons alone contribute to the saturation transfer contrast in brain tumors.

Recently new methods have been proposed to quantify the APT effect and separate it from broad macromolecular MTC, NOE and/or amine protons. These methods fall into two categories. The first class of approaches employs a standard z-spectrum acquisition followed by fitting of individual peaks in the amide and aliphatic regions of the z-spectrum without employing asymmetry assumptions (Jin et al., 2012a; Jones et al., 2012; Zaiss et al., 2011). The second involves specialized acquisition schemes, such as frequency labeled exchange transfer (FLEX) (Friedman et al., 2010), saturation with frequency alternating RF irradiation (SAFARI) (Scheidegger et al., 2011), two frequency RF irradiation (Lee et al., 2012), CEST phase mapping using a length and offset varied saturation scheme (LOVARS) (Song et al., 2012) or chemical exchange rotation transfer (CERT) (Zu et al., 2012a; Zu et al., 2012b).

In this paper, we used a combination of imaging methods including standard z-spectroscopy as a function of irradiation power, low-power z-spectroscopy with fitting of the amide and aliphatic peaks and SAFARI imaging to assess the individual contributions of saturation transfer from amide protons, aliphatic protons, amine protons, and broad macromolecular MTC in human glioma at 3 Tesla.

Methods

Subjects

A total of 14 subjects were recruited for this study. There were six healthy volunteers (4 men, 2 women; median age 43 [range 31–52] years) and eight patients with malignant gliomas (5 men, 3 women; median age 55.5 [range 48–68] years). Tumor locations and pathological findings are described in Table 1. For all patients, diagnosis and grading of disease was confirmed in the Brain Tumor Clinic prior to our examination. Seven of eight subjects had histologically confirmed glioblastoma at initial diagnosis while one had histological diagnosis of malignant astrocytoma with features suggestive of secondary glioblastoma. All were scanned following a protocol approved by our institutional review board and after giving written informed consent. Six of eight subjects had their scans performed at the time of tumor recurrence while two were scanned at initial diagnosis. Patients with recurrent disease had been treated with a combination of surgical resection or biopsy, radiation, cytotoxic chemotherapy, targeted therapy and/or NovoTTF-100A device (Fonkem and Wong 2012; Kirson et al., 2007; Stupp et al., 2012), prior to enrollment in this study. These patients were enrolled in the study after the diagnosis of disease or progression was made clinically and scanned an average of 21 days after their last clinical MRI scan.

Imaging

All studies were performed on a 3 Tesla GE SIGNA HDxt (GE Healthcare, Waukesha WI) whole-body MR scanner. The body coil was used for excitation and a standard eight-channel receive-only head array was used for signal reception.

In the glioma patients, conventional T_2 weighted fluid attenuated inversion recovery (FLAIR: TE/TI/TR = 130/2250/10000 ms, FOV=24cm, slice thickness=5mm, slice spacing = 1.5mm, matrix=320x224, scan time approximately 3.5min) and 3D pulsed continuous arterial spin labeling (Dai et al., 2012; Dai et al., 2008) perfusion images (ASL: labeling duration = 3.5 s, post labeling delay = 1.5s. Stack of spirals RARE readout: 7 spiral interleaves, TE/TR = 10/6952 ms, FOV = 24cm, resolution = 3.35 x 3.35 x 4mm, NEX = 3, scan time approximately 6 min) were acquired to localize the tumor. A single slice passing through a region with intense ASL signal, FLAIR hyperintensity, and with signs of contrast enhancement on the prior clinical scan was selected. Preference was given to slice locations away from regions of greater B_0 nonuniformity. In the healthy volunteers, a single axial slice passing through the superior part of the lateral ventricles was selected.

The off-resonance saturation transfer imaging sequence consisted of continuous wave (CW) RF irradiation [20ms of half Blackman window shaped rise – CW saturation at power B_1 for T_{sat} – 20ms half Blackman window shaped ramp down] followed by a single shot spin-echo EPI acquisition [TR = 2000 ms, TE ranging from 15.8 to 17.4 ms, FOV = 24 cm, matrix = 96 x 96, slice thickness = 8 mm]. By adiabatically ramping up the power to the CW amplitude B_1, the saturation period becomes equivalent to a spin-lock experiment, which minimizes signal oscillations, particularly at short saturation times and high power levels. One unsaturated S_0 image was acquired for reference (NEX=12). Z-spectra were acquired at 32 frequency offsets pairs up to ±5 kHz (0, ±25, ±50, ±100, ±150, ±175, ±200, ±250, ±275,

±300, ±325, ±350, ±375, ±400, ±425, ±450, ±475, ±500, ±525, ±550, ±600, ±700, ±900, ±1200, ±1500, ±2000, ±3000, ±4000, ±5000 Hz). Z-spectra were first acquired with B_1 = 0.5 μT (NEX = 4) and 1.5μT (NEX = 1) and saturation time T_{sat} = 200 ms. This 240 ms CW pulse was the longest permitted by the RF amplifier. The chosen power levels are typical of prior studies focused on saturation transfer from the slow exchanging amide protons. Next, Z-spectra were acquired with B_1 = 3 μT (NEX = 1) and 6 μT (NEX = 1) and T_{sat} = 100 ms. These power levels are more optimal for study of rapidly exchanging lines from amine and hydroxyl protons. The shorter T_{sat} reduces deposited power, the T_{1rho} shortening effects of DS (Jin et al., 2012b) and broad macromolecular MTC, and the contribution from MTC asymmetry (Jin et al., 2012b). Scan time was approximately 2 min per z-spectrum.

To further characterize saturation transfer effects in glioma patients, APT-SAFARI images (Scheidegger et al., 2011) were acquired. The APT-SAFARI imaging sequence consisted of a 3 second pulsed-RF irradiation [Blackman window shaped inversion pulses: pulse width = 9 ms, interpulse delay = 6 ms, equivalent CW power = 0.78 μT] followed by a single shot EPI acquisition [TR = 4000 ms, TE ranging from 15.8 to 17.4 ms, FOV = 24cm, matrix = 96 x 96, slice thickness = 8mm]. One unsaturated S_0 image was acquired for reference followed by twenty-four images for the SAFARI scan: 6 at RF offset = +3.5 ppm, 6 at RF offset = −3.5 ppm and 12 with alternating frequency preparations, interleaved in time. Total scan time was 1.5 minutes.

Image analysis

Image analysis was performed in MATLAB 7.11 (Mathworks, Natick MA). All images were realigned to the first S_0 image using the motion correction algorithm in the SPM8 software package (Wellcome Trust Centre for Neuroimaging, UCL, London). Then, for each acquisition type, images were normalized voxel-by-voxel by the corresponding unsaturated reference image S_0.

For the z-spectrum scans, B_0 correction was performed following the water saturation shift referencing (WASSR) method (Kim et al., 2009): The B_1 = 0.5 μT z-spectrum was fit voxel-by-voxel to a Lorentzian line in the frequency range ±250 Hz only. The fit function was given by (Jones et al., 2012):

$$y = 1 - A \cdot [LW^2/(LW^2 + 4 \cdot (f_0 - x)^2)] + B \quad [3]$$

where LW is the Lorentzian linewidth, f_0 is the center frequency, and A and B are scaling constants. The resulting lineshape was evaluated with a frequency resolution of 1 Hz. The frequency with the minimum fit intensity was assumed to be the center of the water peak. Following the WASSR method, the B_0 map derived from the 0.5 μT z-spectrum was used to correct all of the z-spectra acquired at higher B_1 power. Each z-spectrum was interpolated by a piecewise cubic hermite interpolating polynomial to a resolution of 1 Hz and shifted to center the water frequency at 0 Hz in all voxels. After B_0 correction, the z-spectra were resampled back to their original frequency resolution.

The resulting B_0-corrected images were used to perform standard asymmetry analysis given by:

$$MTR_{asym}=S_{sat}(\omega_-)/S_0-S_{sat}(\omega_+)/S_0 \quad [4]$$

Asymmetry maps at the amide proton frequency were generated by averaging MTR_{asym} across the 425–475 Hz frequency range (referred to as MTR_{asym}(3.5 ppm)). Similarly, asymmetry maps at the amine proton frequency were generated by averaging MTR_{asym} across the 200–350 Hz frequency range (referred to as MTR_{asym}(2 ppm)) Broad macromolecular MTC asymmetry maps were generated by averaging MTR_{asym} across the 1.5–4 kHz frequency range (referred to as MTR_{asym}(20 ppm)). Conventional MTC maps were also generated by averaging $MTR=1-S_{sat}/S_0$ across the −1.5 to −4 kHz frequency range and across the +1.5 to +4 kHz frequency range, referred to as MTR(−20 ppm) and MTR(+20 ppm), respectively.

Following recently published methods (Jin et al., 2012a; Jones et al., 2012), amide and aliphatic proton saturation transfer parameters were also isolated by fitting the low power z-spectrum. Several modifications were made to these high field methods to account for the lower SNR and decreased separation between the amide and aliphatic lines and the water line at 3T. The z-spectrum was constructed voxel-by-voxel from the 0.5 μT acquisition and averaged across specific regions of interest (ROIs) (see below for ROI selection). The resulting mean z-spectrum was interpolated by a piecewise cubic hermite polynomial except at data points around the amide (275 to 650 Hz) and aliphatic (−275 to −700 Hz) frequency ranges. The interpolated z-spectrum was then evaluated at the omitted points in order to calculate the difference between the acquired mean z-spectrum and the interpolated z-spectrum. The amide and aliphatic peaks were characterized by the value of the z-spectrum difference at 3.5 ppm and −3.5 ppm, respectively, and also by integrating the differences across the entirety of the peaks. Integral values were generated by summing the differences multiplied by the step size (25 Hz) across the amide frequency range (275 to 650 Hz) and the aliphatic frequency range (−275 to −700 Hz). Peak integral units are given in Hz.

For the APT-SAFARI scans, quantitative maps of MTR_{SAFARI} were calculated voxel-by-voxel as described previously (Scheidegger et al., 2011):

$$MTR_{SAFARI}=S_{sat}(-3.5\text{ppm})/S_0+S_{sat}(+3.5\text{ppm})/S_0-[S_{sat}(\text{SAFARI})/S_0+S_{sat}(\text{SAFARI}')/S_0] \quad [5]$$

where S_{sat}(SAFARI) is the signal after alternating frequency irradiation and S_{sat}(SAFARI′) is a similar image but with the order of positive and negative frequency reversed to minimize any timing related systematic errors. As the SAFARI method is insensitive to B_0 inhomogeneity up to 200Hz at 3T (Scheidegger et al., 2011), no B_0 correction was performed on the images used to compute MTR_{SAFARI} maps.

In each glioma patient, three ROIs were selected: two in the tumor and one in the normal appearing brain on the contralateral side. Regions were hand drawn on the S_0 images, using the T_2-FLAIR and ASL perfusion from the research scan and T_1 pre and post Gd from the previously acquired clinical scan as guides. Tumor ROIs were drawn in the region with maximum perfusion hyperintensity and in a region with prior contrast enhancement on clinical scans but no current perfusion hyperintensity. The contralateral ROI was drawn

symmetric to the tumor ROIs in the opposite hemisphere, except for one frontal tumor with bilateral extent. For that tumor a region in the occipital lobe was selected as a control. To compare parameters across regions in all patients, statistical analysis was performed by one-way analysis of variance (ANOVA) with Tukey-Kramer test for multiple comparisons. All across subject data are reported as mean ± standard error.

In healthy volunteers, two regions were selected corresponding to white matter and gray matter. The white matter ROI was located laterally in the occipital white matter. The gray matter ROI was placed in the occipital cortex along the midline. Note that due to the relatively low resolution of the echoplanar images, the gray matter ROI may be partially contaminated by both white matter and cerebrospinal fluid. To compare parameters across regions in all healthy volunteers, statistical analysis was performed by paired t-test with Bonferroni correction for multiple comparisons. Data are reported as mean ± standard error.

Simulations

The saturation transfer signal was simulated for a four-pool model (water, amide, amine, MTC) using the analytical solution to the Bloch-McConnell equations presented by Zaiss and Bachert (Zaiss and Bachert 2013). Z-spectra were modeled at RF offsets ranging from −15 to +15ppm with saturation duration T_{sat} = [100, 200, 500, 10000] ms and saturation power B_1 =[0.5, 1.5, 3, 6] μT). Exchange parameters were: proton exchange rates k_{amide} = 30 Hz, k_{amine} = 5000 Hz, k_{MT} = 20Hz; concentrations M_{amide}(brain) = 1/2000M_{0w}, M_{amine}(brain) = 1/120M_{0w}, M_{MT}(brain) = 1/37M_{0w}, M_{amide}(glioma) = 1/1200M_{0w}, M_{amine}(glioma) = 1/120M_{0w}, M_{MT}(glioma) = 1/85M_{0w}; resonance frequencies ω_{amide} = 3.5ppm, ω_{amine} = 2.5ppm, ω_{MT} = −2.3ppm; water relaxation times T_{1w}=1.5s, T_{2w}=70ms; exchangeable amide and amine proton relaxation time T_{2s}=33ms and macromolecular proton relaxation time T_{2MT}=230μs. The exchange parameters above were taken from the literature (Hua et al., 2007b; Liepinsh and Otting 1996; Morrison and Henkelman 1995; Morrison et al., 1995; Wüthrich 1986; Zhou and van Zijl 2006; Zhou et al., 2003b). The concentrations of exchangeable protons in the brain and in glioma were calibrated to match the experimental results. Note that a Lorentzian line, rather than a super-Lorentzian line was used to describe macromolecular exchange. The Lorentzian line provides an accurate description of MTC and removes errors due to the singularity of the super-Lorentzian line when modeling small saturation offsets less than ~15ppm (Morrison and Henkelman 1995; Morrison et al., 1995). The long T_{2MT} = 230 μs reflects the use of the Lorentzian model rather than the super-Lorentzian.

Results

All participants completed the entire study and image quality was acceptable for all studies.

Normal Subject Results

Z-spectra from the healthy volunteers showed the expected features of off-resonance saturation transfer spectroscopy. Broad macromolecular MTC caused increasing attenuation of the image intensity with increasing power and greater attenuation in white matter than gray matter (Figure 1a). At 0.5 μT, both white and gray matter z-spectra showed a narrow

saturation peak at +3.5 ppm consistent with the APT effect. A broader peak on the opposite side of the spectrum that approximately spans the frequency range from −2.2 ppm to −5.5 ppm (Figure 1c) was also observed. This broader peak had previously been attributed to NOE transfer of magnetization from aliphatic protons (Avni et al., 2009; Jin et al., 2012a; Jin et al., 2012b; Jones et al., 2012; Ling et al., 2008; Mori et al., 1998; Mougin et al., 2010; Narvainen et al., 2010; van Zijl et al., 2003; Wüthrich 1986; Zhou et al., 2003b). The amide peak appeared somewhat larger in gray matter than white matter. However, the peak integrals showed no statistically significant tissue contrast in the amide or aliphatic regions (Table 2). At saturation power higher than 0.5 μT, direct water saturation and broad macromolecular magnetization transfer increased along with higher line broadening of the amide and aliphatic peaks, which were no longer identifiable.

The MTR_{asym} curves (Figure 1b) revealed several features. First, there was a large negative asymmetry due to the aliphatic lines and broad macromolecular MTC asymmetry effects. At low RF power ($B_1 \leq 1.5$ μT) this asymmetry peaked close to the water line (offsets < 10 ppm) but remained prominent up to several tens of ppm. The negative asymmetry was maximal at a saturation power of 1.5 μT and was greater in white matter than in gray matter. Second, there was a broad positive amine peak that was most prominent at high saturation power ($B_1 \geq 3$ μT). The peak was centered approximately at 1.6 ppm at 3 μT and 2.7 ppm at 6 μT. The amine peak was much broader and more power dependent than the APT effect, consistent with a faster exchange rate. The shape, amplitude and frequency of the broad amine peak was in very good agreement with the saturation transfer peak reported from amine proton solutions (Haris et al., 2012) and in-vivo studies of amine exchange (Cai et al., 2012; Jin et al., 2012b). Therefore, it can most likely be attributed to fast exchanging amine protons from brain metabolites, other small molecules, and protein and peptide side chains, although an additional contribution from hydroxyl protons cannot be excluded. Third, the APT peak at +3.5 ppm was not seen on the MTR_{asym} curves at any power level as its amplitude was much smaller than that of the negative macromolecular MTC asymmetry and aliphatic proton effects.

Quantitative maps and regional averages (Table 3) mirrored the qualitative impression of the z-spectra. MTR_{asym}(3.5 ppm, 1.5 μT) maps were negative, suggesting a primary contribution to the signal from broad macromolecular MTC asymmetry. They showed significant tissue contrast with white matter being more negative than gray matter ($P = 0.002$). Correspondingly, MTR_{asym}(20 ppm, 1.5 μT) maps showed signal amplitude and contrast very similar to the MTR_{asym}(3.5 ppm, 1.5 μT) map despite being acquired at frequency offsets far away from the amide resonance and other mobile protons. As the power increased from 1.5 μT to 6 μT, broad macromolecular MTC increased while the amplitude of the MTC asymmetry decreased. Note that at 3 μT and 6 μT, the saturation time had been reduced to 100 ms instead of 200 ms. MTR_{asym}(2 ppm, 6 μT) maps were positive, suggesting that the primary contribution to the asymmetry at high power is from saturation transfer of fast exchanging protons rather than broad MTC asymmetry. MTR_{asym}(2 ppm, 6 μT) maps did not show significant tissue contrast.

Glioma results

Z-spectra in the glioma patients (Figure 2) were qualitatively similar to those in the normal subjects. At 0.5 μT, saturation peaks corresponding to amide and aliphatic protons could be seen in the tumor and contralateral regions, similar to those observed in healthy volunteers. The amide peak in the tumor regions appeared increased compared to the contralateral region, while the aliphatic peak appeared decreased. At 3.5ppm, there was a statistically significant increase in the amide peak in the ASL hyperintensity tumor region compared to the contralateral region (Table 4). While the peak integrals showed a trend towards higher values in the tumor regions, statistical analysis did not reveal any differences between regions ($P = 0.07$, Table 4). No statistically significant differences were detected between the peak integral values measured in the contralateral region and those from healthy volunteers.

At higher saturation power, the amide and aliphatic peaks were no longer identifiable by visual inspection, as was observed in healthy volunteers, due to increasing DS, broad macromolecular MTC and line broadening of the amide and aliphatic proton peaks. There was, however, a large decrease in the overall MTC saturation in the tumor regions compared to the contralateral region, which became more prominent as the power increased.

Clear differences between tumor and contralateral tissue were apparent in the MTR_{asym} curves (Figure 3). At low RF power ($B_1 \leq 1.5$ μT), MTR_{asym} was significantly more negative in the normal appearing brain than in the tumor. The difference between MTR_{asym} in the tumor and contralateral regions, ΔMTR_{asym}, was maximal at 1.5 μT and peaked approximately at 3.5 ppm. ΔMTR_{asym} remained prominent at frequency offsets greater than 10 ppm. At high RF power ($B_1 \geq 3$ μT) this difference faded, especially at low frequency offsets, as the positive broad MTR_{asym} line attributed to amine exchange became more dominant. There was minimal difference between the amine line shape and magnitude in tumors and contralateral tissue.

Quantitative maps (Figures 4 and 5) and regional averages (Table 5) confirmed the qualitative impression of the z-spectra. All glioma regions exhibited an elevated MTR_{asym}(3.5 ppm, 1.5 μT), as had been observed in other studies of human high grade brain tumors performed with similar saturation power (Zhao et al., 2011; Zhao et al., 2012). While the normal appearing contralateral brain had negative MTR_{asym}(3.5 ppm, 1.5 μT), tumors had positive values. Similarly, MTR_{asym}(20 ppm, 1.5 μT) was less negative and MTR(+20 ppm) and MTR(−20 ppm) were decreased in all tumors compared to the contralateral brain. In contrast, MTR_{SAFARI} showed no significant differences (Table 4). At higher power, MTR_{asym} (2 ppm, 6 μT) also showed no significant differences between tumors and normal appearing brain. Suggestive small hyperintensities within the tumors on MTR_{SAFARI} maps and MTR_{asym}(2 ppm, 6 μT) maps were observable in two of the patients (one with untreated glioma, one with recurring glioma), e.g. Figure 4, but further studies would be required to establish the significance of such image features. No differences were observed between the 2 patients at initial diagnosis and the 6 patients with recurring tumors.

Simulation results

The MTR_{asym} curves (Figure 6a–d) predicted by the four-pool model were qualitatively very similar to those observed experimentally. At B_1 powers of 0.5 and 1.5μT (T_{sat} = 200 ms), the amide peak was clearly seen along with a negative MTC asymmetry. As the power increased to 3 and 6 μT (T_{sat} = 100 ms), the amide peak was no longer observable and the MTC asymmetry was reduced. At these high power levels, the amine peak was the dominant signal contribution. The contribution of each exchangeable proton to the total signal and glioma contrast can be approximated from two-pool model simulations (Table 6). With the saturation parameters used in this paper, the simulated glioma contrast due to amide protons was ΔAPTR(3.5 ppm, 1.5 μT) ~ 0.16% while the contrast due to the loss of MTC asymmetry was $\Delta MTR'_{asym}$(3.5 ppm, 1.5 μT) ~ 0.86%. Therefore, the bulk of the glioma contrast ΔMTR_{asym}(3.5 ppm, 1.5 μT) = 1.0% given by the four-pool model can be accounted for by a loss of MTC asymmetry. For saturation times T_{sat} = 500 ms, the four-pool model predicted a glioma contrast ΔMTR_{asym}(3.5 ppm, 1.5 μT) = 2.0%. Two-pool model simulations revealed that the contributions to the contrast are approximately the sum of ΔAPTR(3.5 ppm, 1.5 μT) ~ 0.35% and $\Delta MTR'_{asym}$(3.5 ppm, 1.5 μT) ~ 1.61%.

At long saturation time of 10 s, the MTR_{asym} curves showed different features (Figure 6i–l). The amplitude of the slow exchanging amide and negative MTC asymmetry increased dramatically, while the signal due to fast exchanging amine protons was reduced. The four-pool model predicted a maximal glioma contrast at the lowest B_1 power: ΔMTR_{asym}(3.5ppm, 0.5 μT) = 3.6% with amide and MTC contributions ΔAPTR (3.5ppm, 0.5 μT) ~1.16% and $\Delta MTR'_{asym}$(3.5ppm, 0.5 μT) ~ 2.44%, respectively. At higher power, the glioma contrast decreased to ΔMTR_{asym}(3.5ppm, 1.5 μT) = 2.8% with amide and MTC contributions ΔAPTR(3.5ppm, 1.5 μT) ~ 0.70% and $\Delta MTR'_{asym}$(3.5ppm, 1.5 μT) ~ 1.72%, respectively. Therefore, even at long saturation durations optimal for amide proton saturation, simulations predict that about two thirds of the expected glioma contrast could be accounted for by changes in MTC asymmetry rather than amide proton transfer.

Discussion

In this paper, we have obtained saturation transfer measurement at a wide range of frequency offsets in order to assess the individual contributions of saturation transfer from conventional broad macromolecular magnetization transfer contrast and mobile protons such as amide protons, aliphatic protons and amine protons in human glioma tumors at 3T.

Saturation transfer from amide protons, aliphatic protons and broad macromolecular protons in glioma

Our primary finding is that contrast between glioma and normal brain tissue is dominated by broad macromolecular magnetization transfer asymmetry, rather than chemical exchange from mobile protons. At B_1 power less than 2 μT, our study shows a statistically significant increase in MTR_{asym}(3.5 ppm) in the glioma tumors compared to the contralateral brain, as was observed previously with longer saturation times (Jones et al., 2006; Salhotra et al., 2008; Wang et al., 2012; Wen et al., 2010; Zhao et al., 2011; Zhao et al., 2012; Zhou et al.,

2003a; Zhou et al., 2008; Zhou et al., 2011). The contrast in glioma can be modeled in terms of equation [2]:

$$\Delta MTR_{asym} = MTR_{asym}(\text{glioma}) - MTR_{asym}(\text{contralateral}) = \Delta MTR'_{asym} + \Delta APTR$$

From the results in Tables 4 and 5, we derive the following parameters: ΔMTR_{asym}(3.5ppm, 1.5 μT) = 1.20%, ΔAPTR(3.5ppm, 0.5 μT) = 0.17% ≈ ΔAPTR(3.5ppm, 1.5 μT), resulting in a nonzero $\Delta MTR'_{asym}$(3.5ppm, 1.5 μT) = 1.03%. Note that because the saturation efficiency of amide protons is greater than 95% at 0.5 μT (Jones et al., 2012), little additional amide proton saturation is expected when increasing the power from 0.5μT to 1.5μT. Therefore, ΔAPTR(0.5 μT) can be used as a surrogate measure of ΔAPTR(1.5 μT).

In addition, ΔMTR_{asym}(20ppm, 1.5 μT), which should only reflect MTC asymmetry is 0.48%. Modeling of the MTC effect shows that MTC asymmetry is expected to be even larger at 3.5ppm than at 20ppm (Hua et al., 2007b). Therefore, at least half of $\Delta MTR'_{asym}$(3.5ppm) can be accounted for by a loss of MTC asymmetry. By extending the z-spectrum acquisition to high spectral frequencies beyond those of exchangeable protons, our results show that the largest contribution to the signal amplitude and contrast in MTR_{asym} (3.5ppm) can be accounted for by MTC asymmetry, rather than APTR. A decrease in MTC asymmetry in glioma was also reported previously in an animal model (Hua et al., 2007a). Given that MTR_{asym} (20ppm), MTR(+20ppm) and MTR(−20ppm) were all statistically increased in brain tumors, $\Delta MTR'_{asym}$ is a major source of contrast and cannot be assumed to be zero. These results also underscore that ΔMTR_{asym} analysis is not sufficient to accurately quantify the amide proton signal change in tumors (ΔAPTR) since $\Delta MTR'_{asym}$ is a major contributor to the contrast. Alternate acquisition and/or analysis schemes that do not rely on asymmetry analysis must instead be used to accurately assess the APT effect in brain tumors.

Transfer from protons in the aliphatic spectral region appears to make a major contribution to negative z-spectrum asymmetry at lower powers. This finding confirms recent other reports characterizing the aliphatic lines (Jin et al., 2012a; Jones et al., 2012). Since the nature and characteristics of these lines are not well understood, we cannot exclude the possibility that our empirical baseline fitting approach does not appropriately model and quantify these lines. It is clear, however, that they make simple asymmetry analysis inaccurate at low powers because of their overlap with the amide and amine lines, contributing a negative component to MTR′asym(3.5ppm) at low power levels.

Our previously proposed SAFARI technique (Scheidegger et al., 2011) was highly successful at eliminating magnetic field inhomogeneity errors in this clinical population, but it produced relatively little contrast between tumors and normal tissue. Since SAFARI is mostly sensitive to saturable lines, amine and broad MTC contributions should be minimized. The symmetric nature of the saturation should combine the amide and the aliphatic protons contributions. Therefore, similarly to equation [1], we can express the SAFARI contrast as:

$$MTR_{SAFARI}(3.5\text{ppm}) = APTR + AliphaticPTR \quad [6]$$

Since the SAFARI acquisition employs a 3s saturation duration, the APT effect should be much larger than in the z-spectra acquisitions and be near steady-state. Based on the measurements of the amide peak in this paper and extrapolation to longer saturation duration using equation [7], the amide contribution to SAFARI in the healthy brain is likely about 2.1% (see below for more details on the estimates). The roughly 2.5% SAFARI signal observed in the brain is fairly consistent with this estimate but slightly larger, due to the additional positive component of aliphatic contribution to SAFARI. The expected amplitude of the aliphatic contribution to SAFARI with long saturation is difficult to estimate because the physical properties of the aliphatic protons, including T_2, are poorly constrained.

The absence of tumor contrast on the longer saturation time SAFARI images is consistent with the absence of contrast with either the aliphatic or amide line integrals individually as measured at shorter saturation time (Table 4). We note that an increase in the APT effect concurrent with a decrease in the aliphatic PTR could provide an alternate explanation for the lack of SAFARI tumor contrast. To the extent that the aliphatic signal is relatively stable with pathology, the amide contrast in SAFARI could still potentially be a useful diagnostic marker in other disease models.

Chemical exchange saturation transfer of amine protons in glioma

Amine protons from brain metabolites, small molecules, free amino acid and protein and peptide side chains is also a source of endogenous CEST contrast (Cai et al., 2012; Haris et al., 2012; Jin et al., 2012b; Ward et al., 2000; Zhou and van Zijl 2006). In addition to broad macromolecular MTC asymmetry, amine exchange appears to be a major contribution to MTR_{asym} from 2–5 ppm at the powers above 1.5 μT used here. Since several previous studies have been performed with similar high powers (Jones et al., 2006; Wen et al., 2010; Zhao et al., 2011; Zhao et al., 2012) they were likely also measuring a significant amine signal. The combination of this positive amine signal with the negative asymmetry of macromolecular MTC leads to complex CEST signal magnitudes and signs. For example, reports of minimal tissue signal at 2 μT (Zhao et al., 2011) can readily be explained by the cancellation of the negative MTC asymmetry in normal tissue by its amine contribution. Despite its major contribution to the signal, amine exchange did not exhibit significant contrast between tumor and brain tissue. However, several individual patients exhibited hyperintensities in the tumor regions, therefore, it remains uncertain whether amine protons can contribute to the diagnostic value of off-resonance saturation imaging beyond the dominant purely broad macromolecular MT contrast previously reported.

Comparison with previous studies

Many studies have identified promising clinical applications of saturation transfer imaging at 3.5ppm as an imaging biomarker for identifying (Jia et al., 2011; Jones et al., 2006; Salhotra et al., 2008; Wen et al., 2010; Zhao et al., 2012; Zhou et al., 2003a; Zhou et al., 2008), and monitoring treatment response (Wang et al., 2012; Zhou et al., 2011) in brain tumors. While the saturation transfer contrast in brain tumors was originally thought to be

caused by increases in the APT effect, our results offer an alternate interpretation based on a primary contribution to the contrast caused by the loss of broad macromolecular MTC and MTC asymmetry normally found in the healthy brain with only a marginal change in the APT effect. However, care must be taken when comparing our results with other studies as it has been shown here and elsewhere that different saturation schemes, and specifically saturation durations, will change the relative contributions of saturation transfer effects from amide, amine, aliphatic and broad macromolecular protons.

Since this study has employed shorter saturation durations than previous published reports of saturation transfer in brain tumor patients, we can attempt a comparison with the literature by extrapolating our results to longer saturations. In Table 4, we found a higher APTR(3.5ppm) = 0.42±0.05% in tumors than the APTR(3.5ppm) = 0.25±0.03% in the contralateral brain acquired with B_1=0.5 μT and T_{sat} = 200 ms. In addition to the simulation results presented above, APTR can also be modeled as follows (Jones et al., 2012; van Zijl and Yadav 2011; Zhou et al., 2003b; Zhou et al., 2004):

$$APTR = x_s \cdot \alpha \cdot k_{sw} \cdot T_{1w} \cdot (1 - \exp(-T_{sat}/T_{1w})) \quad [7]$$

$$\alpha \approx (\gamma B_1)^2 / ((\gamma B_1)^2 + (k_{sw})^2) \quad [8]$$

where α is the saturation efficiency, k_{sw} is the exchange rate from solute to water, T_{1w} is the longitudinal relaxation time of water and x_s is the concentration of amide protons relative to water protons. If we assume for simplicity that the difference in APTR between brain tumors and normal brain is due only to a difference in amide concentration x_s, while k_{sw} and T_{1w} are unchanged, we can estimate the steady state values for APTR at long saturation time (APTRss). Given T_{1w} = 1.5 s and k_{sw} = 30 Hz, we find APTRss ~ 2.1 % in contralateral brain and APTRss ~ 3.5 % in glioma, giving a maximum tumor contrast ΔAPTRss ~ 1.4 %, independent of saturation power for $B_1 \geq 1$ μT. The estimate for APTRss in the contralateral brain is in very good agreement with recent steady state reports of APTR ~ 1.5–2.5 % in the normal rat brain (Jin et al., 2012a) and APTR ~ 1.4–2.9 % in the normal human brain (Jones et al., 2012). However, the estimate for APTRss in glioma is only approximate because changes in tumor T_{1w} should be taken into account at long saturation times.

Prior reports of saturation transfer contrast in brain tumor patients (Jones et al., 2006; Wen et al., 2010; Zhao et al., 2011; Zhao et al., 2012) typically employed 500 ms saturation at 3 T. At short saturation times of T_{sat} = 500 ms or T_{sat} = 200 ms used in this paper, we found that changes in glioma T_{1w} can be ignored without compromising the APTR estimates calculated below. For T_{sat} = 500 ms, we estimate APTR ~ 0.59% in contralateral brain and APTR~0.99% in tumors, giving ΔAPTR~0.4% for saturation powers $B_1 \geq 1$μT. In addition, given a faster amide exchange rate (Liepinsh and Otting 1996; Liu et al., 2013), for instance k_{sw} = 200 Hz, Eq [7]–[8] yield APTR estimates of 2.7–2.9 % in contralateral brain, 1.6–1.7 % in tumors, giving ΔAPTR~1.1–1.2% for saturation powers B_1=2–3 μT and T_{sat}=500 ms. Since prior brain tumor studies typically report ΔMTR_{asym} values on the order of 2% with these saturation parameters, our results suggest that the contrast previously reported in brain tumors may have been primarily the result of changes in MTR'_{asym} with a smaller

contribution from APTR, as measured in this study. A recent study from some of the authors of these earlier papers used low power z-spectrum fitting and found just weakly reduced APT and aliphatic peak in a single grade III astrocytoma and also attributed previous reports of glioma contrast to combinations of MTC asymmetry and other factors (Jones et al., 2013). A recent careful analysis of long duration saturation studies in an experimental glioma model also reached similar conclusions (Xu et al., 2014).

Since the saturation transfer contrast between tumors and normal tissue has previously been ascribed to an increase in free protein concentration in malignant cells solely based on an assumed major contribution from amide proton exchange (Jones et al., 2006; Wen et al., 2010; Zhou et al., 2003a; Zhou et al., 2008; Zhou et al., 2011), this understanding of contrast is brought into question. Our results show that increases in MTR_{asym} (3.5 ppm, 1.5 μT) in tumors coincide with decreased saturation transfer from broad macromolecular MTC and loss of MTC asymmetry compared to the normal brain (Table 5). The existence of similar contrast (Figures 4 and 5) in the unsubtracted broad macromolecular magnetization transfer ratio at both positive and negative frequencies distant from the exchanging lines of mobile protons suggests that differences in MTR, rather than in its fractional asymmetry, are most responsible for the contrast in brain tumors. Previous studies have also shown that broad macromolecular MTC is altered in glioma (Kurki et al., 1995; Kurki et al., 1996; Lemaire et al., 2000; Okumura et al., 1999; Vonarbourg et al., 2004) with higher MTR in normal brain than in brain tumors and higher MTR in high grade than low grade glioma (Kurki et al., 1995), which was shown to correlate with tumor nuclear density. Since MTR_{asym}(3.5ppm) has previously been shown to be an indicator of tumor recurrence (Wang et al., 2012; Zhou et al., 2011), saturation schemes designed to maximize MTC and MTC asymmetry may further improve the characterization of glioma by asymmetry analysis and make MTR_{asym}(3.5ppm) a clinically viable marker of tumor progression.

Technical Considerations

This study demonstrates that a low power (0.5 μT, T_{sat} = 200 ms) z-spectrum acquisition can successfully identify the amide and aliphatic peaks at 3T, similar to recent higher field results (Jin et al., 2012a; Jones et al., 2012; Jones et al., 2013). However, our results highlight the difficulties of imaging the amide CEST signal. Due to the decreased SNR at 3T compared to higher field strengths, voxel-by-voxel fitting could not be performed reliably without significant noise contamination. Instead, fitting was performed after averaging the z-spectrum over each ROI. The choice of fitting procedure such as the simple baseline fit employed here and in (Jin et al., 2012a), as opposed to the Lorentzian fitting approach used by (Jones et al., 2012; Jones et al., 2013) may lead to differences in the measured amplitude of the amide peaks. Note that our pulse sequence had a short CW saturation of 200 ms and that a longer saturation pulse increasing the amide saturation should be beneficial and could improve the statistical significance of the result.

This study also demonstrates how choice of frequency, power, and duration could be used to separate contrast from different sources. To the extent that MTR or MTC asymmetry is a useful diagnostic marker, this contrast can be obtained without CEST contamination at large frequency offsets. In contrast, the amine component can be emphasized at low frequency

offsets by high power irradiation for short duration (Jin et al., 2012b). This maximizes the fast exchanging amine contribution while minimizing MTC asymmetry and saturation related T_1 shortening. Both these imaging methods demonstrated the capability to create high quality, robust images from clinical patients in quite reasonable scan times. Further research will be needed to fully characterize the diagnostic value of the methods in glioma and other diseases.

Conclusion

Tumor contrast from off-resonance saturation transfer images usually attributed to amide proton transfer and protein concentration is instead the result of MTC and MTC asymmetry differences. While the amide peak is detectable, it is a weak signal that requires careful optimization and analysis to avoid contamination from other sources. A previously reported strategy for measuring the amide signal, SAFARI, demonstrated excellent image quality but showed no contrast in glioma. Amine exchange sensitive imaging showed promise for producing relatively robust and high signal measures of exchanging protons with minimal contamination from other sources when shorter saturations with higher powers are used.

Acknowledgments

NIH Grant Sponsor: Supported in part by the National Institutes of Health through grant CA115745

References

Avni R, Mangoubi O, Bhattacharyya R, Degani H, Frydman L. Magnetization transfer magic-angle-spinning z-spectroscopy of excised tissues. J Magn Reson. 2009; 199(1):1–9. [PubMed: 19409825]

Cai K, Haris M, Singh A, Kogan F, Greenberg JH, Hariharan H, Detre JA, Reddy R. Magnetic resonance imaging of glutamate. Nat Med. 2012; 18(2):302–306. [PubMed: 22270722]

Dai W, Robson PM, Shankaranarayanan A, Alsop DC. Reduced resolution transit delay prescan for quantitative continuous arterial spin labeling perfusion imaging. Magn Reson Med. 2012; 67(5): 1252–1265. [PubMed: 22084006]

Dai W, Garcia D, de Bazelaire C, Alsop DC. Continuous flow-driven inversion for arterial spin labeling using pulsed radio frequency and gradient fields. Magnetic Resonance in Medicine. 2008; 60(6):1488–1497. [PubMed: 19025913]

Fonkem E, Wong ET. NovoTTF-100A: A new treatment modality for recurrent glioblastoma. Expert Rev Neurother. 201210.1586/ERN.12.80

Friedman JI, McMahon MT, Stivers JT, Van Zijl PC. Indirect detection of labile solute proton spectra via the water signal using frequency-labeled exchange (FLEX) transfer. J Am Chem Soc. 2010; 132(6):1813–1815. [PubMed: 20095603]

Haris M, Nanga RP, Singh A, Cai K, Kogan F, Hariharan H, Reddy R. Exchange rates of creatine kinase metabolites: Feasibility of imaging creatine by chemical exchange saturation transfer MRI. NMR Biomed. 2012; 25(11):1305–1309. [PubMed: 22431193]

Henkelman RM, Stanisz GJ, Graham SJ. Magnetization transfer in MRI: A review. NMR Biomed. 2001; 14(2):57–64. [PubMed: 11320533]

Hua J, van Zijl PCM, Sun PZ, Zhou J. Quantitative description of magnetization transfer (MT) asymmetry in experimental brain tumors. Proc Intl Soc Mag Reson Med. 2007a; 15:882.

Hua J, Jones CK, Blakeley J, Smith SA, van Zijl PC, Zhou J. Quantitative description of the asymmetry in magnetization transfer effects around the water resonance in the human brain. Magn Reson Med. 2007b; 58(4):786–793. [PubMed: 17899597]

Jia G, Abaza R, Williams JD, Zynger DL, Zhou J, Shah ZK, Patel M, Sammet S, Wei L, Bahnson RR, et al. Amide proton transfer MR imaging of prostate cancer: A preliminary study. J Magn Reson Imaging. 2011; 33(3):647–654. [PubMed: 21563248]

Jin T, Wang P, Zong X, Kim SG. MR imaging of the amide-proton transfer effect and the pH-insensitive nuclear overhauser effect at 9.4 T. Magn Reson Med. 2012a10.1002/mrm.24315

Jin T, Wang P, Zong X, Kim SG. Magnetic resonance imaging of the amine-proton EXchange (APEX) dependent contrast. Neuroimage. 2012b; 59(2):1218–1227. [PubMed: 21871570]

Jones CK, Schlosser MJ, van Zijl PC, Pomper MG, Golay X, Zhou J. Amide proton transfer imaging of human brain tumors at 3T. Magn Reson Med. 2006; 56(3):585–592. [PubMed: 16892186]

Jones CK, Polders D, Hua J, Zhu H, Hoogduin HJ, Zhou J, Luijten P, van Zijl PC. In vivo three-dimensional whole-brain pulsed steady-state chemical exchange saturation transfer at 7 T. Magn Reson Med. 2012; 67(6):1579–1589. [PubMed: 22083645]

Jones CK, Huang A, Xu J, Edden RA, Schar M, Hua J, Oskolkov N, Zaca D, Zhou J, McMahon MT, et al. Nuclear overhauser enhancement (NOE) imaging in the human brain at 7T. Neuroimage. 2013; 77:114–124. [PubMed: 23567889]

Kim M, Gillen J, Landman BA, Zhou J, van Zijl PC. Water saturation shift referencing (WASSR) for chemical exchange saturation transfer (CEST) experiments. Magn Reson Med. 2009; 61(6):1441–1450. [PubMed: 19358232]

Kirson ED, Dbaly V, Tovarys F, Vymazal J, Soustiel JF, Itzhaki A, Mordechovich D, Steinberg-Shapira S, Gurvich Z, Schneiderman R, et al. Alternating electric fields arrest cell proliferation in animal tumor models and human brain tumors. Proc Natl Acad Sci USA. 2007; 104(24):10152–10157. [PubMed: 17551011]

Kogan F, Singh A, Debrosse C, Haris M, Cai K, Nanga RP, Elliott M, Hariharan H, Reddy R. Imaging of glutamate in the spinal cord using GluCEST. Neuroimage. 2013; 77:262–267. [PubMed: 23583425]

Kurki T, Lundbom N, Komu M, Kormano M. Tissue characterization of intracranial tumors by magnetization transfer and spin-lattice relaxation parameters in vivo. J Magn Reson Imaging. 1996; 6(4):573–579. [PubMed: 8835948]

Kurki T, Lundbom N, Kalimo H, Valtonen S. MR classification of brain gliomas: Value of magnetization transfer and conventional imaging. Magn Reson Imaging. 1995; 13(4):501–511. [PubMed: 7674845]

Lee JS, Regatte RR, Jerschow A. Isolating chemical exchange saturation transfer contrast from magnetization transfer asymmetry under two-frequency rf irradiation. J Magn Reson. 2012; 215:56–63. [PubMed: 22237631]

Lemaire L, Franconi F, Saint-Andre JP, Roullin VG, Jallet P, Le Jeune JJ. High-field quantitative transverse relaxation time, magnetization transfer and apparent water diffusion in experimental rat brain tumour. NMR Biomed. 2000; 13(3):116–123. [PubMed: 10861992]

Liepinsh E, Otting G. Proton exchange rates from amino acid side chains--implications for image contrast. Magn Reson Med. 1996; 35(1):30–42. [PubMed: 8771020]

Ling W, Regatte RR, Navon G, Jerschow A. Assessment of glycosaminoglycan concentration in vivo by chemical exchange-dependent saturation transfer (gagCEST). Proc Natl Acad Sci USA. 2008; 105(7):2266–2270. [PubMed: 18268341]

Liu D, Zhou J, Xue R, Zuo Z, An J, Wang DJJ. Quantitative characterization of nuclear overhauser enhancement and amide proton transfer effects in the human brain at 7 tesla. Magnetic Resonance in Medicine. 2013; 70(4):1070–1081. [PubMed: 23238951]

Mori S, Eleff SM, Pilatus U, Mori N, van Zijl PC. Proton NMR spectroscopy of solvent-saturable resonances: A new approach to study pH effects in situ. Magn Reson Med. 1998; 40(1):36–42. [PubMed: 9660550]

Morrison C, Henkelman RM. A model for magnetization transfer in tissues. Magn Reson Med. 1995; 33(4):475–482. [PubMed: 7776877]

Morrison C, Stanisz G, Henkelman RM. Modeling magnetization transfer for biological-like systems using a semi-solid pool with a super-lorentzian lineshape and dipolar reservoir. J Magn Reson B. 1995; 108(2):103–113. [PubMed: 7648009]

Mougin OE, Coxon RC, Pitiot A, Gowland PA. Magnetization transfer phenomenon in the human brain at 7 T. Neuroimage. 2010; 49(1):272–281. [PubMed: 19683581]

Narvainen J, Hubbard PL, Kauppinen RA, Morris GA. Z-spectroscopy with alternating-phase irradiation. J Magn Reson. 2010; 207(2):242–250. [PubMed: 20920868]

Okumura A, Takenaka K, Nishimura Y, Asano Y, Sakai N, Kuwata K, Era S. The characterization of human brain tumor using magnetization transfer technique in magnetic resonance imaging Neurol. Res. 1999; 21(3):250–254.

Pekar J, Jezzard P, Roberts DA, Leigh JS Jr, Frank JA, McLaughlin AC. Perfusion imaging with compensation for asymmetric magnetization transfer effects. Magn Reson Med. 1996; 35(1):70–79. [PubMed: 8771024]

Salhotra A, Lal B, Laterra J, Sun PZ, van Zijl PC, Zhou J. Amide proton transfer imaging of 9L gliosarcoma and human glioblastoma xenografts. NMR Biomed. 2008; 21(5):489–497. [PubMed: 17924591]

Scheidegger R, Vinogradov E, Alsop DC. Amide proton transfer imaging with improved robustness to magnetic field inhomogeneity and magnetization transfer asymmetry using saturation with frequency alternating RF irradiation (SAFARI). Magn Reson Med. 2011; 66(5):1275–1285. [PubMed: 21608029]

Song X, Gilad AA, Joel S, Liu G, Bar-Shir A, Liang Y, Gorelik M, Pekar JJ, van Zijl PC, Bulte JW, et al. CEST phase mapping using a length and offset varied saturation (LOVARS) scheme. Magn Reson Med. 2012; 68(4):1074–1086. [PubMed: 22246684]

Stein, AD.; Roberts, DA.; McGowan, J.; Reddy, R.; Leigh, JS. Asymmetric cancellation of magnetization transfer effects. Proceedings SMR, 2nd Annual Meeting; San Fransisco. 1994. p. 880

Stupp R, Wong ET, Kanner AA, Steinberg D, Engelhard H, Heidecke V, Kirson ED, Taillibert S, Liebermann F, Dbaly V, et al. NovoTTF-100A versus physician's choice chemotherapy in recurrent glioblastoma: A randomised phase III trial of a novel treatment modality. Eur J Cancer. 2012; 48(14):2192–2202. [PubMed: 22608262]

van Zijl PC, Yadav NN. Chemical exchange saturation transfer (CEST): What is in a name and what isn't? Magn Reson Med. 2011; 65(4):927–948. [PubMed: 21337419]

van Zijl PC, Zhou J, Mori N, Payen JF, Wilson D, Mori S. Mechanism of magnetization transfer during on-resonance water saturation. A new approach to detect mobile proteins, peptides, and lipids. Magn Reson Med. 2003; 49(3):440–449. [PubMed: 12594746]

Vonarbourg A, Sapin A, Lemaire L, Franconi F, Menei P, Jallet P, Le Jeune JJ. Characterization and detection of experimental rat gliomas using magnetic resonance imaging. MAGMA. 2004; 17(3–6):133–139. [PubMed: 15503254]

Wang S, Tryggestad E, Zhou T, Armour M, Wen Z, Fu DX, Ford E, van Zijl PC, Zhou J. Assessment of MRI parameters as imaging biomarkers for radiation necrosis in the rat brain. Int J Radiat Oncol Biol Phys. 2012; 83(3):e431–6. [PubMed: 22483739]

Ward KM, Aletras AH, Balaban RS. A new class of contrast agents for MRI based on proton chemical exchange dependent saturation transfer (CEST). J Magn Reson. 2000; 143(1):79–87. [PubMed: 10698648]

Wen Z, Hu S, Huang F, Wang X, Guo L, Quan X, Wang S, Zhou J. MR imaging of high-grade brain tumors using endogenous protein and peptide-based contrast. Neuroimage. 2010; 51(2):616–622. [PubMed: 20188197]

Wolff SD, Balaban RS. Magnetization transfer contrast (MTC) and tissue water proton relaxation in vivo. Magn Reson Med. 1989; 10(1):135–144. [PubMed: 2547135]

Wüthrich, K. NMR of proteins and nucleic acids. Wiley; New York: 1986.

Xu J, Zaiss M, Zu Z, Li H, Xie J, Gochberg DF, Bachert P, Gore JC. On the origins of chemical exchange saturation transfer (CEST) contrast in tumors at 9.4T. NMR Biomed. 2014; 27(4):406–416. [PubMed: 24474497]

Zaiss M, Schmitt B, Bachert P. Quantitative separation of CEST effect from magnetization transfer and spillover effects by lorentzian-line-fit analysis of z-spectra. J Magn Reson. 2011; 211(2):149–155. [PubMed: 21641247]

Zaiss M, Bachert P. Exchange-dependent relaxation in the rotating frame for slow and intermediate exchange ? modeling off-resonant spin-lock and chemical exchange saturation transfer. NMR Biomed. 2013; 26(5):507–518. [PubMed: 23281186]

Zhao X, Wen Z, Huang F, Lu S, Wang X, Hu S, Zu D, Zhou J. Saturation power dependence of amide proton transfer image contrasts in human brain tumors and strokes at 3 T. Magn Reson Med. 2011; 66(4):1033–1041. [PubMed: 21394783]

Zhao X, Wen Z, Zhang G, Huang F, Lu S, Wang X, Hu S, Chen M, Zhou J. Three-dimensional turbo-spin-echo amide proton transfer MR imaging at 3-tesla and its application to high-grade human brain tumors. Mol Imaging Biol. 201210.1007/s11307-012-0563-1

Zhou J, van Zijl PCM. Chemical exchange saturation transfer imaging and spectroscopy. Progr NMR Spectr. 2006; 48:109–136.

Zhou J, Wilson DA, Sun PZ, Klaus JA, Van Zijl PC. Quantitative description of proton exchange processes between water and endogenous and exogenous agents for WEX, CEST, and APT experiments. Magn Reson Med. 2004; 51(5):945–952. [PubMed: 15122676]

Zhou J, Lal B, Wilson DA, Laterra J, van Zijl PC. Amide proton transfer (APT) contrast for imaging of brain tumors. Magn Reson Med. 2003a; 50(6):1120–1126. [PubMed: 14648559]

Zhou J, Payen JF, Wilson DA, Traystman RJ, van Zijl PC. Using the amide proton signals of intracellular proteins and peptides to detect pH effects in MRI. Nat Med. 2003b; 9(8):1085–1090. [PubMed: 12872167]

Zhou J, Blakeley JO, Hua J, Kim M, Laterra J, Pomper MG, van Zijl PC. Practical data acquisition method for human brain tumor amide proton transfer (APT) imaging. Magn Reson Med. 2008; 60(4):842–849. [PubMed: 18816868]

Zhou J, Tryggestad E, Wen Z, Lal B, Zhou T, Grossman R, Wang S, Yan K, Fu DX, Ford E, et al. Differentiation between glioma and radiation necrosis using molecular magnetic resonance imaging of endogenous proteins and peptides Nat. Med. 2011; 17(1):130–134.

Zu Z, Janve VA, Xu J, Does MD, Gore JC, Gochberg DF. A new method for detecting exchanging amide protons using chemical exchange rotation transfer. Magn Reson Med. 2012a10.1002/mrm.24284

Zu Z, Janve VA, Li K, Does MD, Gore JC, Gochberg DF. Multi-angle ratiometric approach to measure chemical exchange in amide proton transfer imaging. Magn Reson Med. 2012b; 68(3):711–719. [PubMed: 22161770]

Highlights

We describe robust methods to measure chemical exchange saturation transfer (CEST)

We separated amine and amide CEST effects from magnetization transfer (MT) asymmetry

We measured CEST and MT asymmetry signal in patients with recurrent glioma.

MT asymmetry is mostly responsible for the contrast between glioma and normal Brain

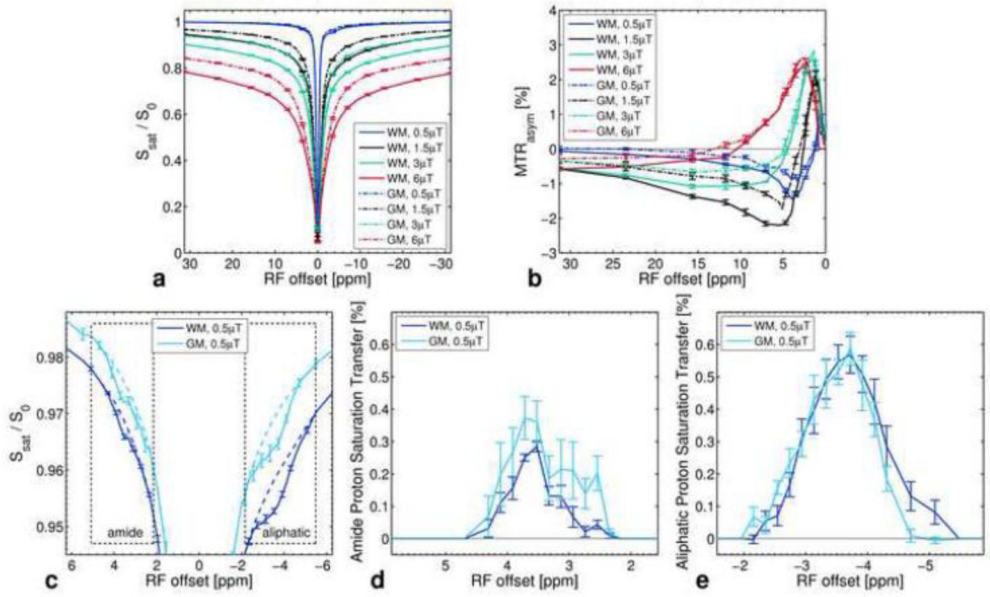

Figure 1.

Saturation transfer data in healthy volunteers. a) The z-spectrum derived from occipital white matter (WM) and gray matter (GM) ROIs in healthy volunteers (N = 6) as a function of saturation power. b) MTR_{asym} shows a large negative asymmetry, which is more prominent in white matter than gray matter. The amide peak at +3.5ppm is not observed, but a CEST peak from faster exchanging protons, centered in the 2–3 ppm range, can be seen at high power. c) A close up of the amide and aliphatic regions of the z-spectrum acquired at 0.5 μT shows saturation peaks centered at +3.5 ppm and approximately −3.7 ppm respectively. The amplitude of the amide and aliphatic peaks were quantified by the difference between the z-spectrum fit (dotted lines) and the acquired data (solid lines) integrated over the frequency ranges delimited by the black boxes. Corresponding line shapes and amplitudes for d) the amide and e) the aliphatic spectral regions. The peaks represent the remainder after subtracting the interpolated fit to the z-spectrum excluding these points from the original 0.5 μT z-spectrum data. In subfigures a)-c) error bars are only shown for a subset of acquired data points for clarity.

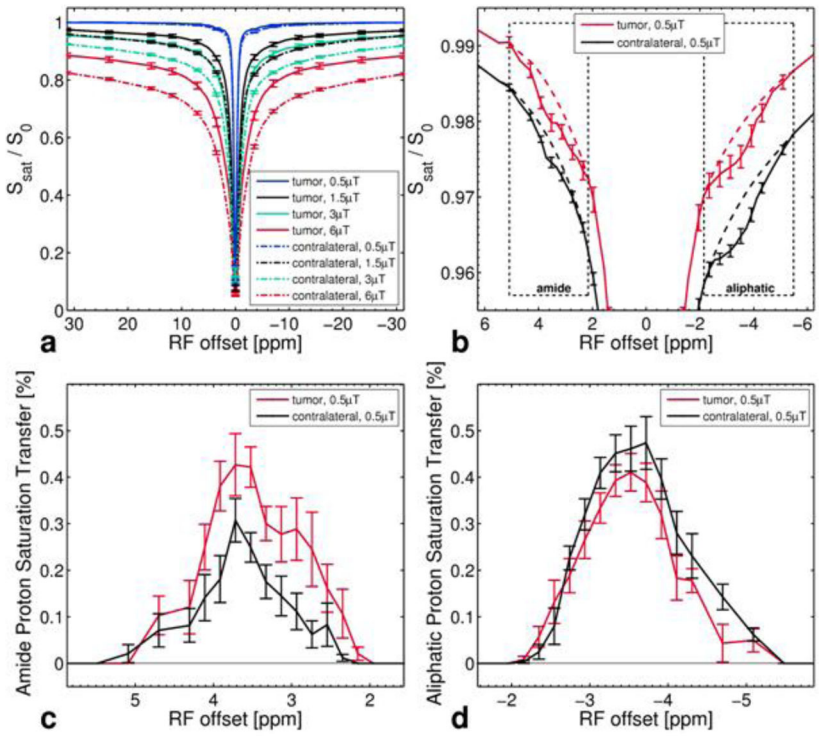

Figure 2.

Saturation transfer data in glioma. a) The z-spectrum derived from the ASL hyperintensity tumor region and the contralateral region in glioma patients (N = 8) as a function of saturation power. For simplicity, the contrast enhancing ROI is not shown as both tumor ROIs overlap on this scale. b) A close up of the amide and aliphatic regions of the z-spectrum acquired at 0.5 μT shows saturation peaks centered at +3.5 ppm and approximately −3.5 ppm respectively. Line shapes and amplitudes for c) the amide and d) the aliphatic spectral regions represent the remainder after subtracting the interpolated fit to the z-spectrum excluding these points from the original 0.5 μT z-spectrum data. In panels a) and b) error bars are only shown for a subset of acquired data points for clarity.

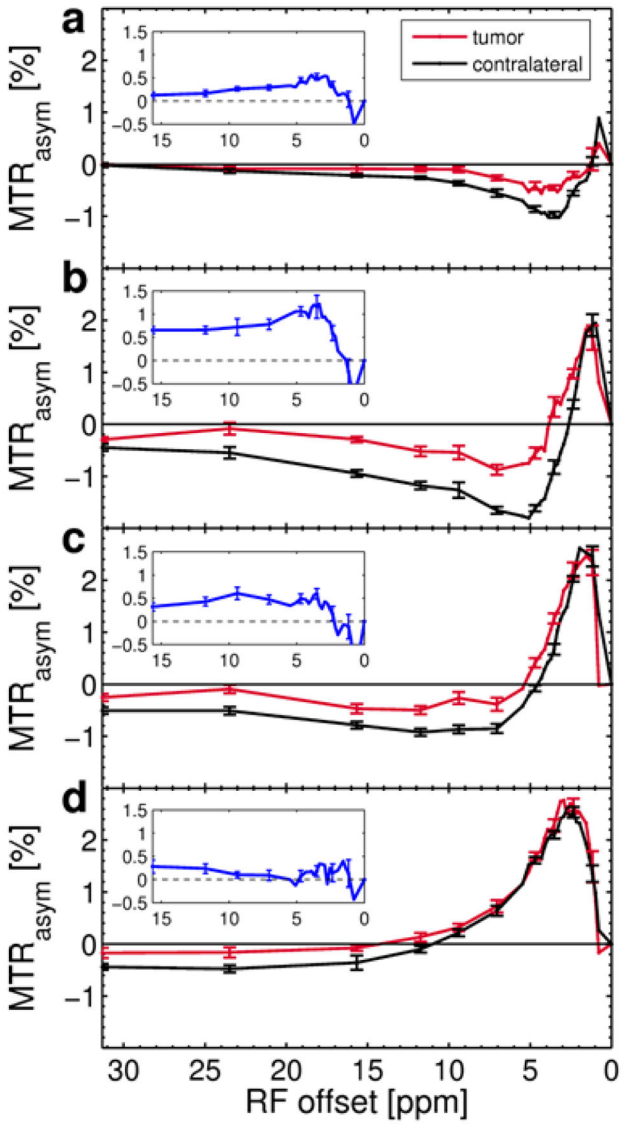

Figure 3.

MTR_{asym} vs. saturation power in glioma (N=8). a) B_1 = 0.5 μT, b) B_1 = 1.5 μT, c) B_1 = 3.0 μT, d) B_1 = 6.0 μT. The insets show ΔMTR_{asym} between the tumor and contralateral region. Error bars are only shown for a subset of acquired data points for clarity.

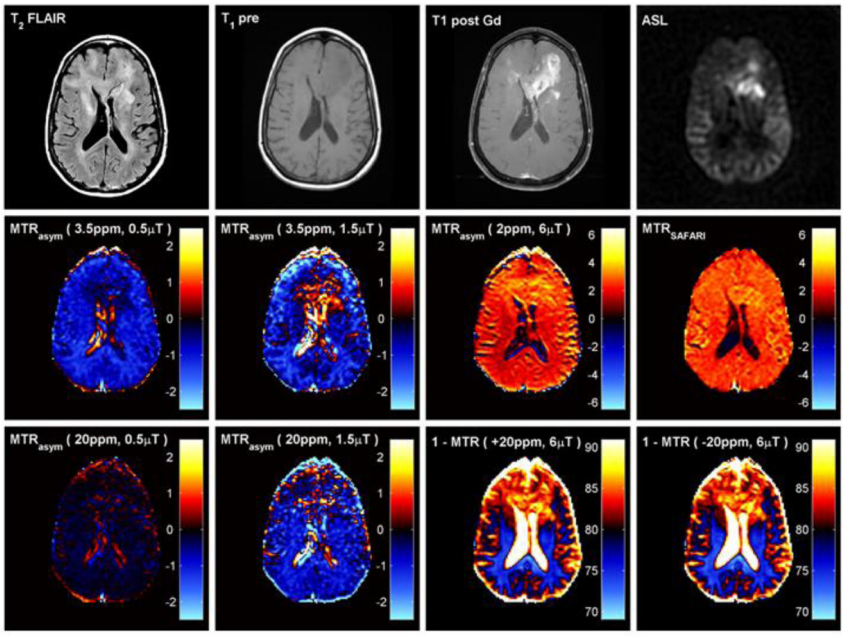

Figure 4.

Saturation transfer maps compared with several other types of standard MR images for a patient with an untreated glioblastoma.

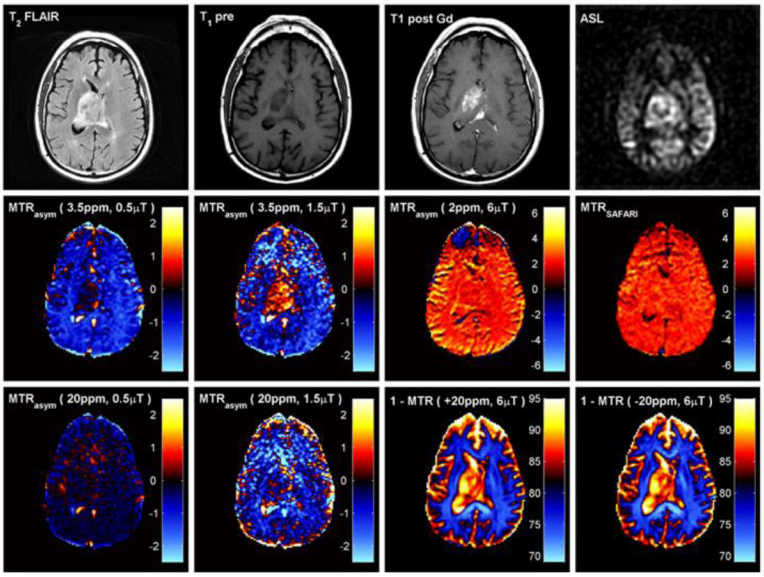

Figure 5.

Saturation transfer maps compared with several other types of standard MR images for a patient with an astrocytoma.

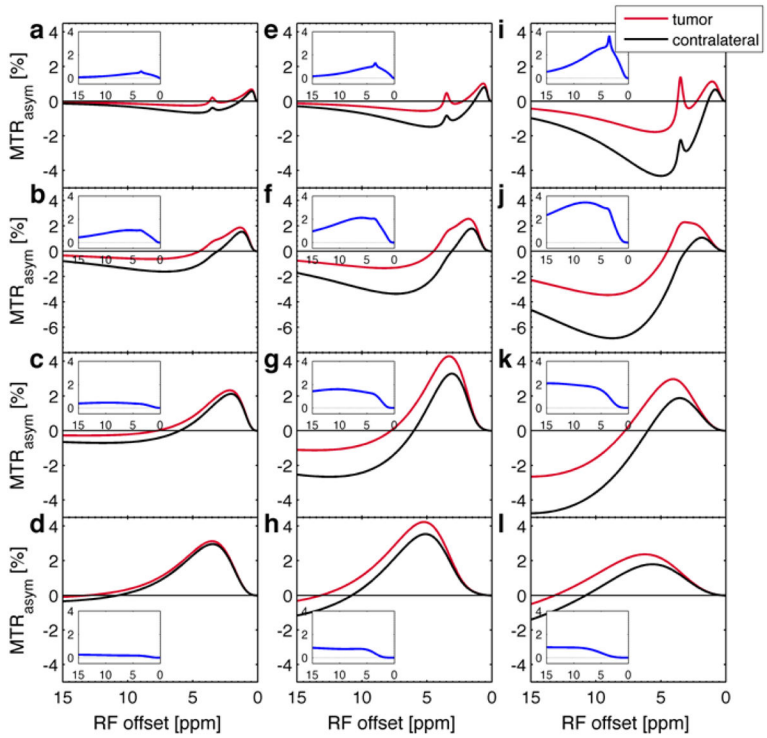

Figure 6.

Simulated MTR_{asym} vs. saturation power and duration for a four-pool model consisting of water, amide, amine and macromolecular exchange. Left column: Simulation with experimental saturation parameters: a) B_1 = 0.5 μT, T_{sat} = 200 ms, b) B_1 = 1.5 μT, T_{sat} = 200 ms, c) B_1 = 3.0 μT, T_{sat} = 100 ms, d) B_1 = 6.0 μT, T_{sat} = 100 ms. Middle column: Simulation with moderate saturation duration T_{sat} = 500 ms: e) B_1 = 0.5 μT, f) B_1 = 1.5 μT, g) B_1 = 3.0 μT, h) B_1 = 6.0 μT. Right column: Simulation with long saturation duration T_{sat} = 10 s: i) B_1 = 0.5 μT, j) B_1 = 1.5 μT, k) B_1 = 3.0 μT, l) B_1 = 6.0 μT. The insets show ΔMTR_{asym} between the tumor and contralateral region.

Table 1

Pathology report and clinical management of the 8 glioma patients scanned.

Number	Sex	Age	Pathology	Lesion Location	Prior treatment and interventions
1	M	48	Glioblastoma, WHO Grade 4	Left parieto-occipital, left temporal lobes	Biopsy, temozolomide chemo-irradiation Additional treatments: adjuvant monthly temozolomide[a] (1 cycle), dose-dense temozolomide[b] (1 cycle), bevacizumab (5 cycles), lomustine (1 cycle), daily etoposide (1 cycle), irinotecan (1 cycle), and NovoTTF-100A (2 cycles)
2	M	53	Glioblastoma, WHO Grade 4	Left occipital mass with recurrence in left parietal lobe	Gross total resection, temozolomide chemo-irradiation Additional chemotherapy: adjuvant monthly temozolomide[a] (12 cycles)
3	F	57	Glioblastoma, WHO Grade 4	Bi-frontal mass with extension across the genu of the corpus callosum	Biopsy
4	F	65	Glioblastoma, WHO Grade 4	Right parietal mass with recurrence in right frontal lobe	Gross total resection, temozolomide chemo-irradiation Additional chemotherapy: adjuvant monthly temozolomide[a] (1 cycle) and bevacizumab (1 cycle)
5	M	54	Malignant astrocytoma (probable secondary glioblastoma)	Right thalamus	Biopsy, ventriculostomy, proton beam radiation therapy
6	M	49	Glioblastoma, WHO Grade 4	Right frontal lobe, centrum semiovale	Partial resection
7	M	57	Glioblastoma, WHO Grade 4	Left parietal mass with recurrence in left occipital and temporal lobes	Partial resection, temozolomide chemo-irradiation Additional chemotherapy: adjuvant monthly temozolomide[c] (13 cycles)
8	F	68	Glioblastoma, WHO Grade 4	Right parieto-occipital, and 2 left frontal masses	Biopsy, temozolomide chemo-irradiation Additional chemotherapy: adjuvant monthly temozolomide[d] (1 cycle)

[a] Monthly temozolomide at a dose of 200 mg/m^2/day x 5 days in 28-day cycle.

[b] Dose-dense temozolomide at a dose of 150 mg/m^2/day, 7 days on and 7 days off, in 28-day cycle.

[c] Monthly temozolomide at a dose of 390 mg/m^2/day x 5 days in 28-day cycle.

[d] Monthly temozolomide at a dose of 150 mg/m^2/day x 5 days in 28-day cycle.

Table 2

Amide and aliphatic peak integrals derived from the 0.5 μT z-spectrum in healthy volunteers (N = 6) with standard errors. All values were statistically different from zero (P < 0.02). No differences were found between white matter and gray matter regions.

	Amide peak integral [Hz]	Aliphatic peak integral [Hz]	Amide peak at 3.5ppm [%]	Aliphatic peak at −3.5ppm [%]
WM	0.31 ± 0.03	1.01 ± 0.15	0.28 ± 0.02	0.55 ± 0.06
GM	0.56 ± 0.17	0.96 ± 0.09	0.36 ± 0.07	0.51 ± 0.04

Table 3

MTR_{asym} and MTR as a function of saturation power in healthy volunteers (N = 6)

Saturation transfer parameters derived from white matter (WM) and gray matter (GM) regions with standard errors across N=6 healthy volunteers. (†) represent statistically significant differences between WM and GM.

	0.5 μT	1.5 μT	3 μT	6 μT
MTR_{asym} (2ppm) [%]				
WM	−0.72 ± 0.02 †	0.65 ± 0.07	2.23 ± 0.08	2.20 ± 0.07
GM	−0.45 ± 0.04 †	0.96 ± 0.12	2.34 ± 0.11	2.41 ± 0.08
MTR_{asym} (3.5ppm) [%]				
WM	−1.36 ± 0.04 ††	−1.26 ± 0.06 †	0.81 ± 0.04	2.14 ± 0.05
GM	−0.86 ± 0.05 ††	−0.35 ± 0.14 †	1.12 ± 0.10	2.31 ± 0.12
MTR_{asym} (20ppm) [%]				
WM	−0.24 ± 0.01	−1.08 ± 0.02 ††	−0.87 ± 0.04 ††	−0.41 ± 0.02
GM	−0.08 ± 0.05	−0.62 ± 0.06 ††	−0.52 ± 0.05 ††	−0.15 ± 0.06
MTR(+20ppm) [%]				
WM	0.48 ± 0.01	8.05 ± 0.22 ††	13.20 ± 0.25 ††	26.49 ± 0.39 ††
GM	0.36 ± 0.04	4.92 ± 0.16 ††	8.41 ± 0.25 ††	19.41 ± 0.29 ††
MTR(−20ppm) [%]				
WM	0.72 ± 0.01 †	9.13 ± 0.22 ††	14.07 ± 0.28 ††	26.91 ± 0.39 ††
GM	0.44 ± 0.04 †	5.55 ± 0.17 ††	8.93 ± 0.27 ††	19.56 ± 0.33 ††

† $P < 0.04$

†† $P < 0.008$

Table 4

Peak integrals derived from the 0.5 μT z-spectrum and SAFARI parameters in glioma patients (N=8) with standard errors. (†) represent statistically significant differences between tumor and contralateral regions. No statistically significant differences were found between the two tumor regions, or between tumor and contralateral for the peak integrals and the MTR_{SAFARI} parameters.

	Amide peak integral [Hz]	Aliphatic peak integral [Hz]	Amide peak at 3.5ppm [%]	Aliphatic peak at −3.5ppm [%]	MTR_{SAFARI} [%]
ASL hyperintensity	0.78 ± 0.12	0.74 ± 0.09	0.42 ± 0.05 †	0.41 ± 0.04	2.52 ± 0.14
Gd enhancement	0.72 ± 0.13	0.88 ± 0.09	0.31 ± 0.04	0.44 ± 0.04	2.33 ± 0.15
Contralateral	0.41 ± 0.08	0.89 ± 0.08	0.25 ± 0.03	0.46 ± 0.05	2.36 ± 0.04

† Regions statistically different from contralateral $P < 0.02$

Table 5

MTR_{asym} and MTR as a function of saturation power in glioma patients (N = 8)

Saturation transfer parameters derived from tumor regions (ASL hyperintensity and Gd enhancement) and from contralateral normal appearing brain with standard errors across N=8 glioma patients. (†) represent statistically significant differences between tumor and contralateral regions. No statistically significant differences were found between the two tumor regions.

	0.5 μT	1.5 μT	3 μT	6 μT
MTR_{asym} (2ppm) [%]				
ASL hyperintensity	−0.23 ± 0.06 ††	1.17 ± 0.13 †	2.18 ± 0.15	2.54 ± 0.14
Gd enhancement	−0.28 ± 0.05 ††	1.02 ± 0.11	2.02 ± 0.10	2.45 ± 0.14
Contralateral	−0.51 ±0.02	0.65 ± 0.06	2.13 ± 0.07	2.36 ± 0.10
MTR_{asym} (3.5ppm) [%]				
ASL hyperintensity	−0.48 ± 0.05 †††	0.31 ± 0.16 †††	1.24 ± 0.10 ††	2.33 ± 0.12
Gd enhancement	−0.49 ± 0.07 †††	0.17 ± 0.21 †††	1.04 ± 0.07††	2.18 ± 0.16
Contralateral	−0.98 ± 0.06	−0.89 ± 0.10	0.73 ± 0.08	2.13 ± 0.04
MTR_{asym} (20ppm) [%]				
ASL hyperintensity	−0.07 ± 0.02 †	−0.30 ± 0.05 †††	−0.33 ± 0.05 †††	−0.07 ± 0.06†
Gd enhancement	−0.05 ± 0.03†	−0.34 ± 0.08 †††	−0.41 ± 0.06 †††	−0.10 ± 0.08†
Contralateral	−0.15 ± 0.02	−0.78 ± 0.06	−0.68 ± 0.03	−0.35 ± 0.05
MTR(+20ppm) [%]				
ASL hyperintensity	0.14 ± 0.03†	3.75 ± 0.58†	6.09 ± 0.69 ††	14.10 ± 1.02 †††
Gd enhancement	0.15 ± 0.05 †	3.81± 0.72†	5.93 ± 0.94 ††	13.84 ± 1.39 †††
Contralateral	0.30 ± 0.02	6.09 ± 0.26	10.24 ± 0.32	21.38 ± 0.51
MTR(−20ppm) [%]				
ASL hyperintensity	0.20 ± 0.04 †††	4.05 ± 0.62†	6.42 ± 0.70 ††	14.17 ± 1.031 †††
Gd enhancement	0.20 ± 0.04 †††	4.15 ± 0.73†	6.34 ± 0.96 ††	13.94 ± 1.37 †††
Contralateral	0.45 ± 0.02	6.87 ± 0.28	10.92 ± 0.33	21.73 ± 0.50

† Regions statistically different from contralateral $P < 0.02$

†† Regions statistically different from contralateral $P < 0.001$

††† Regions statistically different from contralateral $P < 0.0001$

Table 6

Simulation of MTR_{asym}(3.5ppm) as a function of saturation power and saturation duration in glioma

Simulated saturation transfer parameters at 3.5 ppm modeled for tumor and contralateral normal appearing brain as a function of saturation power and saturation duration. Exchange parameters were: proton exchange rates k_{amide} = 30 Hz, k_{amine} = 5000 Hz, k_{MT} = 20Hz; concentrations M_{amide}(contralateral) = 1/2000M_{0w}, M_{amine}(contralateral) = 1/120M_{0w}, M_{MT}(contralateral) = 1/37M_{0w}, M_{amide}(glioma) = 1/1200M_{0w}, M_{amine}(glioma) = 1/120M_{0w}, M_{MT}(glioma) = 1/85M_{0w}; resonance frequencies ω_{amide} = 3.5ppm, ω_{amine} = 2.5ppm, ω_{MT} = −2.3ppm; water relaxation times T_{1w}=1.5s, T_{2w}=70ms; exchangeable amide and amine proton relaxation time T_{2s}=33ms and macromolecular proton relaxation time T_{2MT}=230μs. Proton concentrations were calibrated against experimental results.

	T_{sat} = 200 ms		T_{sat} = 100 ms		T_{sat} = 500 ms				T_{sat} = 10,000 ms			
	0.5 μT	**1.5 μT**	**3 μT**	**6 μT**	**0.5 μT**	**1.5 μT**	**3 μT**	**6 μT**	**0.5 μT**	**1.5 μT**	**3 μT**	**6 μT**
two-pool model water-amide												
MTR_{asym}(glioma)	0.41	0.42	0.19	0.10	0.93	0.88	0.56	0.14	2.96	1.77	0.51	0.07
MTR_{asym}(contralateral)	0.25	0.25	0.11	0.06	0.56	0.53	0.34	0.08	1.80	1.07	0.31	0.04
ΔMTR_{asym}	0.17	0.17	0.07	0.04	0.37	0.35	0.22	0.05	1.16	0.70	0.20	0.03
two-pool model water-MT												
MTR_{asym}(glioma)	−0.33	−0.70	−0.19	−0.04	−0.74	−1.43	−0.54	−0.05	−2.27	−2.41	−0.43	−0.03
MTR_{asym}(contralateral)	−0.76	−1.57	−0.43	−0.09	−1.68	−3.04	−1.10	−0.11	−4.71	−4.13	−0.77	−0.05
ΔMTR_{asym}	0.43	0.86	0.24	0.05	0.93	1.61	0.56	0.05	2.44	1.72	0.34	0.03
two-pool model water-amine												
MTR_{asym}(glioma)												
MTR_{asym}(contralateral)	0.13	1.06	1.77	3.15	0.29	2.17	4.69	2.98	0.93	3.79	3.44	1.46
four-pool model water-amide-MT-amine												
MTR_{asym}(glioma)	0.21	0.74	1.73	3.13	0.46	1.46	4.25	2.75	1.34	2.11	2.82	1.36
MTR_{asym}(contralateral)	−0.38	−0.31	1.39	2.96	−0.84	−0.58	3.12	2.39	−2.28	−0.69	1.88	1.19
ΔMTR_{asym}	0.59	1.04	0.34	0.17	1.30	2.03	1.13	0.37	3.62	2.80	0.94	0.17